A New THD Measurement Method With Small Computational Burden Using a SOGI-FLL Grid Monitoring System

José Matas, Helena Martín, Jordi de la Hoz, Abdullah Abusorrah, *Senior Member, IEEE*, Yusuf Al-Turki, *Senior Member, IEEE*, and Hamed Alshaeikh

***Abstract*—This article proposes a new method for obtaining the total harmonic distortion (THD) using few math operations, a low-pass filter (LPF), and a grid monitoring system able to provide the fundamental and harmonics components of the grid voltage. The method is particularly developed by using the second-order generalized integrator (SOGI) error signal notch filter transfer function characteristics of a standard SOGI-FLL monitoring system. The method is accurate and has a small computational burden, so it is suitable for the online assessment of the grid voltage or current THD and can easily be implemented into a digital signal processor. The accuracy and transient response of the system have been analyzed, showing that they can easily be determined by the tuning of the SOGI filter and the LPF. The method also shows to be robust to grid perturbations, such us voltage sags, or swells, and frequency step changes. Simulations and experimental results are provided to validate the proposed THD method. Moreover, comparison with a fast Fourier transform (FFT)-based THD is also presented, which shows that the proposed THD method results to be faster, more accurate, and simpler than the FFT-based one.**

***Index Terms*—Digital signal processor (DSP), power quality, THD online measurement, total harmonic distortion (THD).**

I. Introduction

THE TOTAL harmonic distortion (THD) is an important indicator to assess the quality in power systems. The THD measures the deviation of a given signal from an ideal sinusoidal pattern and can be applied to voltages and currents. In electrical systems, the supply voltage can be distorted by the interaction of consumer's nonlinear loads through the impedance of the network. The distortion can induce adverse problems, such as heating of induction motors, distribution transformers and neutral conductors, the erratic operation of breakers and relays, torque pulsations in motors and generators, or the malfunction of sensitive electronic equipment. Moreover, this phenomenon can be amplified by resonance with the capacitors of power factor correction systems, which can push harmonic voltage distortion to unacceptable levels [1], [2]. To reduce these adverse effects, the IEEE standard 519-1992 provides recommended values to limit the harmonic distortion [3]. This document sets limits on voltage harmonics in low-voltage networks to 5% THD, and to a 3% THD in the case of a single harmonic. These limits, in practice, are not enforced, and, therefore, in some systems, the THD content could be found to be much higher.

An online THD measurement of the grid voltage with low computational needs could be interesting in grid monitoring applications to give the ability of controlling online the distortion levels at different parts of the electrical network. It could also be used to monitor the quality of the currents absorbed by the consumer-side loads and for the detection of the use of nonlinear loads due to its specific high THD profile. For microgrids, it could be employed for the detection of nonlinear loads and to improve the quality in the grid-connected and island mode operations. Therefore, such possibility could help in improving the quality of the power system and reducing the distortion levels.

There are few proposals in literature regarding the THD calculation, which can be grouped into frequency or time domains. In [4], a fast Fourier transform (FFT) and discrete Fourier transform (DFT) THD methods were proposed to better exploit the digital signal processor (DSP) accumulator capability for improving the THD calculation precision. In [5], two different THD definitions were examined in order to avoid possible ambiguity and misinterpretation in the measurement. In [6], an analytic THD calculation of nonsinusoidal signals with known Fourier coefficients filtered by bandpass filters (BPF) and using a Cauchy method of residues was proposed. In [7], a DFT variant under a nonsynchronized sampling condition that approximates the fundamental frequency and improves the THD calculation is presented. In [8], an FFT and short-time Fourier transform (STFT) for calculating the THD were proposed. In [9], an analytic algebraic method for obtaining the THD in multilevel inverters considering higher order harmonics and formulating line voltage with unequal dc sources is proposed. In [10], a THD method using a matrix method that maps the measured

Manuscript received March 5, 2019; revised May 5, 2019 and July 18, 2019; accepted October 30, 2019. Date of publication November 17, 2019; date of current version February 20, 2020. This work was supported by the Deanship of Scientific Research (DSR) at King Abdulaziz University, Jeddah, under Grant D-185-135-1440. Recommended for publication by Associate Editor X. Ruan. *(Corresponding author: José Matas.)*

J. Matas, H. Martín, and J. de la Hoz are with the Department of Electric Engineering, Technical University of Catalonia (EEBE-UPC), Barcelona 08019, Spain (e-mail: jose.matas@upc.edu; m.helena.martin@upc.edu; jordi.de.la.hoz@upc.edu).

A. Abusorrah, Y. Al-Turki, and H. Alshaeikh are with the Department of Electrical and Computer Engineering, Faculty of Engineering and the Center of Research Excellence in Renewable Energy and Power Systems, King Abdulaziz University, Jeddah 21589, Saudi Arabia (e-mail: aabusorrah@kau.edu.sa; yaturki@yahoo.com; hamed_1460@yahoo.com).

Color versions of one or more of the figures in this article are available online at http://ieeexplore.ieee.org.

Digital Object Identifier 10.1109/TPEL.2019.2953926

harmonics into a vector of pseudoharmonics was proposed. In [11], a THD calculation based on analog operational amplifiers to implement Fliege BPF was proposed. This method took only into consideration the second and third harmonics and needed manual adjustments due to mistuning of the electronic amplifiers. In [12], an analytical method for deriving the THD of the current of a single-phase multilevel inverter with an *LCL* filter in a grid-connected case was presented. In [13], an analytical expression for the standard THD valid for the case of using estimators with sine fitting was proposed.

In general, these proposals required the calculation of the harmonic components of the signal using spectral analysis, which supposes a considerable computational charge to perform an online measurement of the THD and for being implemented into a DSP [4], [6]–[8]. Other proposals [9], [11]–[13] consist of analytical solutions that provide specific formulas for the THD calculation that can be used under certain conditions and for specific converter topologies. They give insights into the causes of distortions and help to mitigate them through the design of the converter, but cannot be used for an online THD determination of arbitrary signals. Moreover, these publications provide results in which the accuracy of the obtained THD is assessed, but they neither show its dynamic behavior nor how it changes temporally as the signal distortion evolves with time.

This article proposes a new and simple method for obtaining the THD from the fundamental and harmonic components provided by any existing adaptive notch filter (ANF) [14], adaptive BPF as those based on second-order generalized integrator (SOGI) approaches [15]–[18], or PLL-based proposals, such as the SOGI-PLL or EPLL [19]–[22]. The method provides the THD value but without requiring the calculation of any particular harmonic component, or performing any spectral analysis. Although the method could be applied, in general, to any grid monitoring scheme, in this article, it is developed using the well-known SOGI-FLL proposal, for the sake of simplicity. The SOGI-FLL is, in general, a valuable tool employed to estimate the phase, frequency, and amplitude of the grid voltage with low computational needs. Here, the notch filter (NF) transfer function of the SOGI error signal regarding the input signal is used for providing the grid harmonic components, whereas the fundamental component is obtained by means of the orthogonal outputs of the SOGI filter.

The THD is calculated using few math operations: a square of the error signal, a low-pass filter (LPF) to obtain its average, a square root, and a division. The accuracy of the obtained THD relies mainly on the SOGI NF ability, which is determined by its damping factor parameter. The proposed method is simple and can help the existing grid monitoring approaches to incorporate the THD of the grid and monitor its temporal progression through time. The method might also be used to measure the current distortion drawn by the user-side loads and for the detection of nonlinear loads, which could help the network operators to visualize and manage the grid distortion and to develop new ways of limiting their adverse effects and increase the quality of the grid.

Simulations and experimental results are provided to prove that the method is accurate and robust in face of grid voltage faults, such as voltage sags and phase jumps. Moreover, the method is experimentally compared with an alternative online FFT-based THD in a simple test for the detection of a fifth-harmonic distortion. The FFT is implemented into a Texas Instruments (TI) DSP using an FFT optimized software library provided by this manufacturer [24]. The results show that the proposed THD achieves faster and better results than the FFT-based one and behaves better when the grid frequency deviates from the nominal 50 Hz value. The results also show that the computational load is very small compared with the FFT.

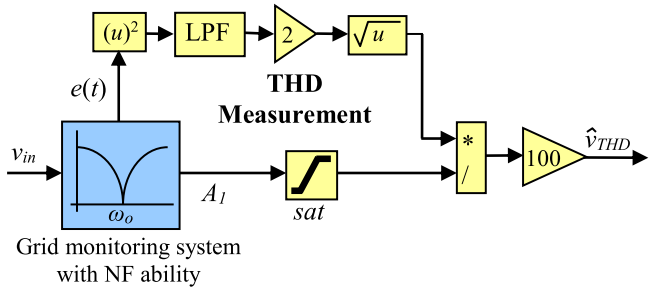

Fig. 1. Block diagram of the proposed THD measurement method.

This article is organized as follows. Section II exposes the proposed THD measurement method for being generally applied to any grid monitoring system. Section III develops the method by using the SOGI-FLL approach. A detailed analysis of the system accuracy, dynamic behavior, and robustness in front of grid perturbations is provided in this section. Section IV provides experimental results for validating the proposal and compares it with an alternative FFT-based proposal. Section V concludes this article.

II. THD Measurement Method

Fig. 1 depicts the scheme of the proposed THD measurement method, which is composed by few blocks: a general grid monitoring system with NF ability, an LPF, and few math operations.

The method calculates the THD according to the standard definition presented in [1] and [2], which define the THD as the square root of the sum of the squared harmonic components of a given signal divided by the fundamental component

$$\mathrm{THD} = \frac{\sqrt{\sum_h |A_h|^2}}{A_1} \cdot 100 \tag{1}$$

where h is the harmonic order, A_h is the amplitude of the hth harmonic component, with $h \neq 1$, and A_1 is the amplitude of the fundamental component. The grid monitoring system should be able to provide an estimate of A_1 and the rest of harmonic components contained in a given signal, named as $e(t)$ in this case. A periodic single-phase input signal v_{in} without dc component and containing only the odd harmonic components that are usually present in the grid voltage is considered for sake of simplicity, i.e., $h = 3, 5, 7, \ldots$ Therefore, v_{in} can be described as follows:

$$v_{\mathrm{in}}(t) = A_1 \sin(\omega_i t) + \sum_h A_h \sin(h\omega_i t + \phi_h) \tag{2}$$

where ω_i is frequency of the grid, and φ_h is the phase angle of the *h*th harmonic component. The harmonic components can be extracted by the NF capability that some grid monitoring approaches have. Then, the signal $e(t)$ can be identified with the second term of (2), i.e.,

$$e(t) \cong \sum_h A_h \sin\left(h\omega_i t + \phi_h\right). \tag{3}$$

The square operation over $e(t)$ will produce

$$e^2(t) \approx \sum_h A_h^2 \sin^2\left(h\omega_i t + \phi_h\right) + \sum_h \sum_{k,k\neq h} A_h A_k \sin\left(h\omega_i t + \phi_h\right) \sin\left(k\omega_i t + \phi_k\right). \tag{4}$$

Therefore, the square operation generates the square of every harmonic in (2) plus a family of products between the harmonics. Using trigonometric identities, (4) can be expressed as follows:

$$e^2(t) \approx \sum_h \frac{A_h^2}{2}\left[1 - \cos(2h\omega_i t + 2\phi_h)\right] + \sum_h \sum_{k,k\neq h} \frac{A_h A_k}{2}[\cos((h-k)\omega_i t + \phi_h - \phi_k) - \cos((h+k)\omega_i t + \phi_h + \phi_k)]. \tag{5}$$

Also, from (5), it can be seen that finally a dc component is generated that is equal to the sum of the square of the amplitude of all the harmonic components in (3) affected by a 1/2 gain, plus a series of double frequency harmonic components, and plus an additional series of sinusoidal components. The last ones are components that pulsate at frequencies equal to the sum $(h + k)$ and to the difference $(h - k)$, which result from the family of multiplications between harmonics in (4).

In (5), it is important to see that the relevant part corresponds to the dc component, which is directly the sum of the square of all the harmonic components and can be used to obtain the THD of (1) without the need of complex calculations. This dc component can be easily extracted from (5) by applying an LPF with a suitable cutoff frequency that can be designed to remove, or mitigate, the harmonic components. The LPF achieves the average value of (5), which corresponds to the dc component and can be expressed as follows:

$$\rho = \mathrm{LPF}(e^2) = \langle e^2 \rangle = \sum_h \frac{A_h^2}{2} \tag{6}$$

where $< >$ represents the averaged value. The performance of the averaged value relies on the LPF cutoff frequency. Furthermore, the LPF can be of second-, third-, or *n*th-order for the better and accurate removal of the oscillating components.

Finally, according to Fig. 1, the THD is obtained by multiplying (6) by 2 to cancel the 1/2 gain and by applying the square root, dividing by the fundamental amplitude A_1 and multiplying by 100

$$\mathrm{THD} = \frac{\sqrt{2\rho}}{A_1} \cdot 100. \tag{7}$$

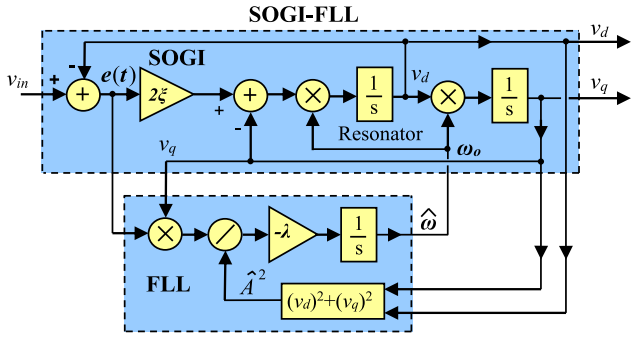

Fig. 2. SOGI-FLL block diagram.

Note that the multiplication by 100 is only necessary to calculate the value in a percentage scale. In Fig. 1, the obtained THD is denoted as $\hat{v}_{\mathrm{THD}}$, and a saturation block is used to avoid a division by zero. The saturation is set to a small lower boundary that only has effect at the start-up transient.

Fig. 1 depicts a general scheme that might be developed using any of the several reported methods to extract the grid information based either on phase locked loop (PLL), on ANF, or on adaptive BPF as the SOGI-FLL. However, in this article, the method is developed by using the SOGI-FLL due to its simplicity and well-known characteristics.

III. THD Development Using the SOGI-FLL

In this section, the proposed THD method is developed using the SOGI-FLL monitoring system [12]–[15], in order to check its dynamic and accuracy performance under normal and grid distorted conditions. After that, the THD accuracy regarding the NF capability of the SOGI and also the effect of the nonlinearity of the square root operator in the THD dynamic response are analyzed.

A. Development Using the SOGI-FLL Grid Monitoring System

Fig. 2 depicts the block diagram of a SOGI-FLL grid monitoring system. In this figure, the SOGI consists of a frequency-adjustable resonator that is regulated with gain 2ξ for having the output v_d in-phase with the input v_{in} [12]. The resonator is formed by two integrators with the particularity of providing a second output v_q in quadrature phase with v_{in}. The frequency locked loop (FLL) is a simple gradient descent algorithm that adaptively tunes the system with the frequency of v_{in} using the SOGI error e and output v_q [13]–[15].

From the input-to-output point of view, the SOGI error signal $e(t)$ has an NF closed-loop transfer function

$$H_e(s) = \frac{e\,(s)}{v_{\mathrm{in}}\,(s)} = \frac{s^2 + \omega_o^2}{s^2 + 2\xi\omega_o \cdot s + \omega_o^2} \tag{8}$$

where ω_o is the central frequency, and ξ is the damping factor that determines the NF capability. The NF behavior of $e(t)$ is used to provide the harmonic components of the grid voltage, as expressed in (3). The Bode plot of (8) is depicted in Fig. 3 for $\xi = 0.7$ in order to see the NF behavior.

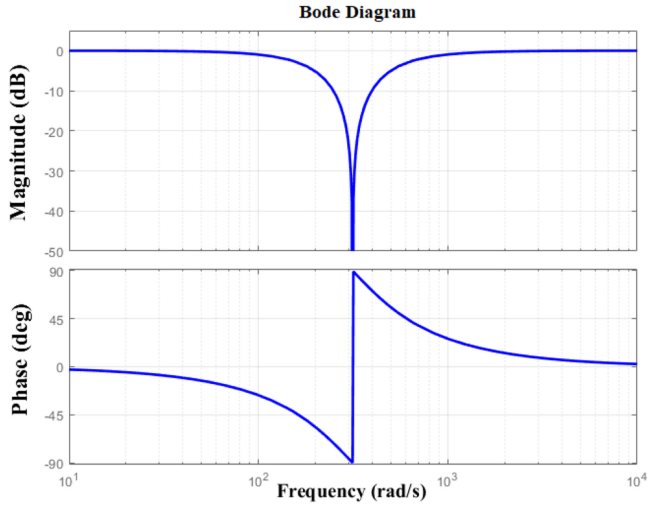

Fig. 3. Bode plot of $H_e(s)$ for $\xi = 0.7$ and $\omega_o = 2\pi 50$ rad/s.

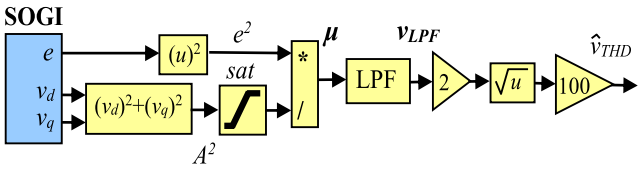

Fig. 4. THD simplified block diagram using the SOGI filter.

The fundamental component of the grid voltage is estimated from the SOGI in-phase v_d and quadrature-phase v_q outputs as

$$\hat{A} = A = \sqrt{v_d^2 + v_q^2} \tag{9}$$

where the estimated fundamental, $\hat{A}$, will, hereafter, be denoted now on as A. The outputs v_d and v_q have the following BPF and LPF transfer function relationship regarding the input

$$\boldsymbol{H_d}(\boldsymbol{s}) = \frac{\boldsymbol{v_d}(\boldsymbol{s})}{\boldsymbol{v_{in}}(\boldsymbol{s})} = \frac{2\boldsymbol{\xi\omega_o}\cdot\boldsymbol{s}}{\boldsymbol{s}^2 + 2\boldsymbol{\xi\omega_o}\cdot\boldsymbol{s} + \boldsymbol{\omega_o^2}} \tag{10}$$

$$\boldsymbol{H_q}(\boldsymbol{s}) = \frac{\boldsymbol{v_q}(\boldsymbol{s})}{\boldsymbol{v_{in}}(\boldsymbol{s})} = \frac{2\boldsymbol{\xi}\omega_o^2}{\boldsymbol{s}^2 + 2\boldsymbol{\xi\omega_o}\cdot\boldsymbol{s} + \boldsymbol{\omega_o^2}}. \tag{11}$$

The FLL estimates the grid frequency from the product between e and v_q and uses the division by the square of (9) to normalize the frequency from the grid amplitude voltage [13]–[15]. The FLL can be expressed as follows:

$$\frac{d\hat{\omega}}{dt} = -\frac{\lambda}{A^2}\cdot e\cdot v_q \tag{12}$$

where $\hat{\omega}$ is the estimated frequency, and λ is the FLL gain. Now, due to availability of the square of A^2 in (9) and in Fig. 2, in this case, the THD of (7) is simplified to

$$\text{THD} = \sqrt{\frac{2}{A^2}\text{LPF}\left(e^2\right)}\cdot 100 = \sqrt{2\cdot\text{LPF}\left(\mu\right)}\cdot 100 \tag{13}$$

where $\mu = e^2/A^2$. And, the corresponding block diagram is shown in Fig. 4.

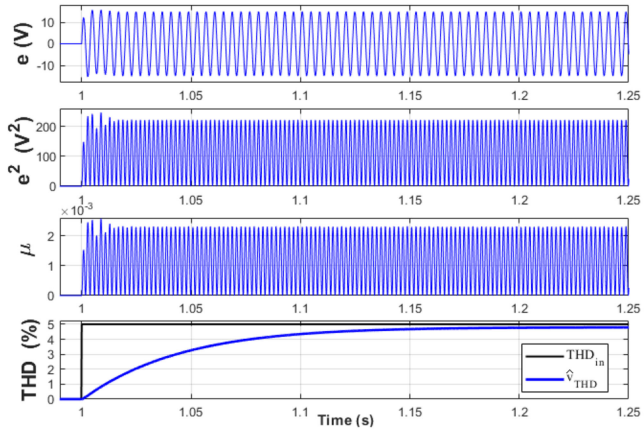

Fig. 5. THD system transient responses to a grid voltage with a fifth harmonic with 5% amplitude that appears at $t_0 = 1$ s.

B. THD Transient Behavior

The system dynamic behavior for an input signal that suffers a sudden step-type THD change corresponds mainly to the dynamics of the LPF, since the harmonic perturbation goes almost unaffected to the SOGI error output and enters into the THD measurement method via the square operation, $e^2(t)$. Considering a single-phase grid voltage with a fifth-harmonic step perturbation at $t = t_0$

$$v_{\text{in}}(t) = A_1\sin(\omega_i t) + A_5\sin(\omega_i t)\cdot u(t - t_0). \tag{14}$$

The perturbation goes to the LPF as

$$\mu(t) = \left(\frac{A_5\cdot|H_e(j5\omega_o t)|}{A}\right)^2\sin^2(5\omega_i t)\cdot u(t - t_0) \tag{15}$$

where $|H_e(j5\omega_o t)|$ is the SOGI NF gain at the fifth harmonic and $\omega_o = \omega_i$.

Fig. 5 depicts the system time response to a harmonic with 5% amplitude that appears at $t_0 = 1$ s. The SOGI and LPF parameters are $\xi = 0.7$, $\omega_o = \omega_i = 2\pi 50$ rad/s, $n = 2$, and $f_c = 5$ Hz, where n is the LPF order and f_c is its cutoff frequency. Note that, in this figure, the harmonic is transformed from bipolar, in $e(t)$ to a unipolar signal, in $e^2(t)$, pulsating at high frequency, which for the LPF, in μ, resembles like a step-like type of input perturbation. Thus, μ is filtered by the LPF and as seen in the bottom subplot, the dynamic response is of exponential type, which corresponds to the LPF dynamics.

Additionally, Fig. 6 illustrates the time response for a combination of 5th, 7th and 11th harmonics with 5% amplitude each, appearing all at $t_0 = 1$ s. Note that the harmonics can be seen in the μ subplot and that the THD response still has an exponential shape. The measured THD amplitudes are 4.8% for Fig. 5 and 8.45% for Fig. 6, which implies a 4% and a 2.43% measurement error, respectively. These errors are due to the SOGI NF impact to the harmonic amplitude voltages, which respectively are affected by the following gains: 0.96, 0.98, and 0.99. For Figs. 5 and 6, the measured THD settling times correspond to the LPF, i.e., $t_s(2\%) = 4/\alpha$, where $\alpha = 2\pi f_c$ (rad/s).

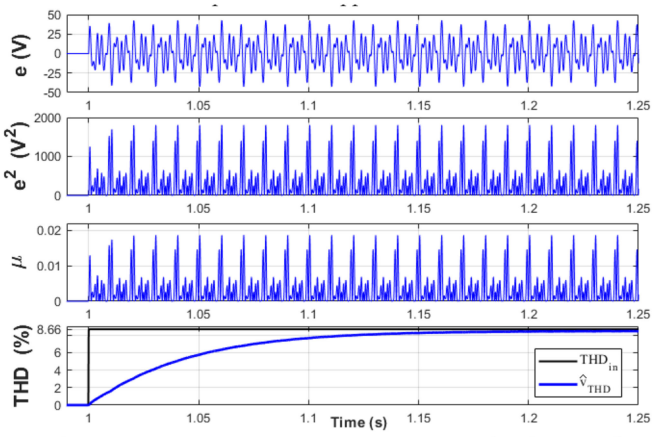

Fig. 6. THD system transient responses to a grid voltage with a combination of 5th, 7th, and 11th harmonics with 5% amplitude each that appears at $t_0 = 1$ s.

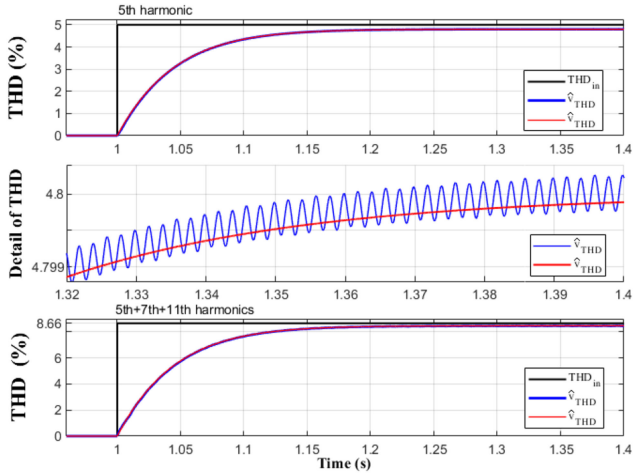

Fig. 7. THD transient response to a grid voltage with two types of harmonics with 5% amplitude each that appear at $t = 1$ s. Top: for a single 5th harmonic. Middle: detail of the single 5th-harmonic case. Bottom: for a combination of 5th, 7th, and 11th harmonics.

As shown in Figs. 5 and 6, the THD dynamic follows an exponential response, which mainly is due to the LPF. The LPF averages μ achieving the summation of the squares of the harmonic components, with each harmonic affected by the square of the SOGI NF gain. That is, at steady state, the LPF output can be expressed as follows:

$$v_{\mathrm{LPF}} = \frac{1}{A^2}\sum_h \frac{A_h^2|H_{e_h}|^2}{2} \approx \frac{1}{2}\left(\frac{1}{A^2}\sum_h A_h^2\right)\cdot\Phi$$
$$= \frac{1}{2}(\mathrm{THD_{in}})^2\cdot\Phi \tag{16}$$

where $H_{e_h} = |H_e(jh\omega_i t)|$ is the SOGI NF magnitude gain at the hth harmonic, $\mathrm{THD_{in}}$ is the THD input harmonic amplitude, and Φ represents the error produced in the measurement due to the H_{e_h} NF factor. At steady state, (16) is multiplied by 2, followed by an sqrt() operator, so the estimated THD is given as follows:

$$\hat{v}_{\mathrm{THD}} = \mathrm{THD_{in}}\cdot\sqrt{\Phi}. \tag{17}$$

And the dynamic behavior at v_{LPF} for a THD step-type input perturbation is described as

$$v_{\mathrm{LPF}}(s) = \frac{1}{2}\left(\frac{\alpha}{s+\alpha}\right)^n \Phi\cdot\frac{(\mathrm{THD_{in}})^2}{s}. \tag{18}$$

Note that, in this case, the expression of the transfer function using directly the THD output $\hat{v}_{\mathrm{THD}}$ has not been addressed in order to avoid difficulties in the Laplace transform definition due to the square root operator. Moreover, sqrt() has a nonlinear gain effect on a step perturbation that is not straightforward to determine and that is analyzed in detail in Section III-C. Nevertheless, for assessing the dynamical behavior of $\hat{v}_{\mathrm{THD}}$, Fig. 7 shows the comparison between the THDs of Figs. 5 and 6, plotted in blue, with that achieved using (18) and considering the square root operator, plotted in red, i.e., $\hat{v}_{\mathrm{THD}} = \sqrt{2\cdot v_{\mathrm{LPF}}(t)}\cdot 100$. A detail is also provided in the middle subplot that proves that (18) perfectly matches the obtained responses shown in Figs. 5 and 6.

C. Accuracy of the System

The measurement accuracy is determined by two factors: the SOGI NF capability for extracting harmonic components in $e(t)$ and the distortion induced by harmonics through v_d and v_q BPF and LPF transfer functions, respectively, in the calculation of A, (9)–(11). The accuracy can be analyzed using the SOGI e, v_d, and v_q magnitude gains regarding the input signal, that from (8), (10) and (11) are

$$|H_e(j\omega_i)| = \left|1-(\omega_i/\omega_o)^2\right|/D, \tag{19}$$
$$|H_d(j\omega_i)| = 2(\omega_i/\omega_o)/D, \tag{20}$$
$$|H_q(j\omega_i)| = 2/D \tag{21}$$

where

$$D = \sqrt{\left[1-(\omega_i/\omega_o)^2\right]^2 + [2(\omega_i/\omega_o)]^2}.$$

And defining $h = \omega_i/\omega_i$ (19)-(21) can be expressed as

$$|H_e(jh\omega_o)| = \left|1-h^2\right|/D2, \tag{22}$$
$$|H_d(jh\omega_o)| = 2h/D2, \tag{23}$$
$$|H_q(jh\omega_o)| = 2/D2 \tag{24}$$

where

$$D2 = \sqrt{[1-h^2]^2 + [2\xi h]^2}.$$

For $e(t)$, the magnitude of (22) can be simplified to $|H_e(jh\omega_o)| \cong 1$ for $h \geq 5$, since $h^2 \gg 2\xi h$ for $h \geq 5$. This means that the THD is quite accurate for $h \geq 5$ and that the THD method is appropriate for three-phase systems. However, for $h < 5$, the harmonics are significantly attenuated for increasing values of the SOGI damping factor ξ. This fact can be seen in Fig. 8 in which the relationship between $|H_e(jh\omega_o)|$ in (20) and ξ is plotted for $h = 3$, 5, 7, and 11.

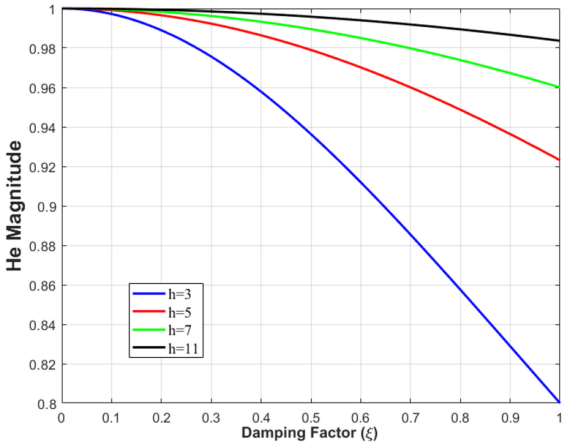

Fig. 8. Plot of $|H_e(jh\omega_o)|$ versus ξ for harmonic orders $h = 3$, 5, 7, and 11.

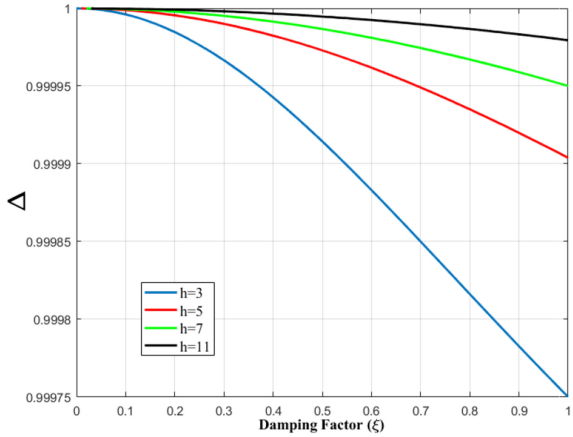

Fig. 9. Plot of Δ versus ξ for harmonic orders $h = 3$, 5, 7, and 11.

In Fig. 8, the highest $|H_e|$ attenuations are also obtained for the highest ξ. So, for $\xi = 1$, the 3rd, 5th, 7th, and 11th harmonics will be affected by the attenuation factors 0.2, 0.08, 0.04, and 0.0164, respectively. However, $|H_e|$ can be adjusted to a desired level by simply reducing ξ. For instance, using Fig. 8 or (22), for $h = 5$, the attenuation can be limited to only 1% by choosing $\xi = 0.34$.

The accuracy can further be analyzed assuming a grid voltage with a single-harmonic component

$$v_{in}(t) = A_1 \sin\theta + A_h \sin\theta_h \tag{25}$$

where $\theta = \omega_i t$ and $\theta = h\omega_i t + \varphi_h$ are the phases of the fundamental and harmonic components, respectively. Assuming that the SOGI is tuned to the input frequency ($\omega_o = \omega_i$). The outputs e, v_d, and v_q are given as follows:

$$e(t) = A_h|H_e|\sin\theta_{he} \tag{26}$$

$$v_d(t) = A_1\sin\theta + A_h|H_d|\sin\theta_{hd} \tag{27}$$

$$v_q(t) = -A_1\cos\theta - A_h|H_q|\cos\theta_{hd} \tag{28}$$

where $|H_e| = |H_e(jh\omega_o)|$, $|H_d| = |H_d(jh\omega_o)|$, $|H_q| = |H_q(jh\omega_o)|$, $\theta_{he} = h\omega_i t + \psi_e$, $\theta_{hd} = h\omega_i t + \psi_d$, $\psi_e = \angle H_e(jh\omega_o)$, and $\psi_d = \angle H_d(jh\omega_o)$. And, the square of A in (9) can be expressed as follows:

$$A^2 = A_1^2 + A_h^2|H_d|^2\sin^2(\theta_{hd}) + A_h^2|H_q|^2\cos^2(\theta_{hd}) + 2A_1A_h \times |H_d|\sin\theta\cdot\sin\theta_{hd} + 2A_1A_1|H_q|\cos\theta\cdot\cos\theta_{hd} \tag{29}$$

which, considering that (24) can be simplified to $|H_q| = |H_d|/h$ and using trigonometric identities, leads to

$$\text{THD} = \sqrt{2\cdot\left\langle \frac{\frac{1}{2}A_h^2|H_e|^2(1-\tilde{q})}{A_1^2 + j + \tilde{r} + \tilde{u}}\right\rangle}\cdot 100 \tag{30}$$

where $< >$ is the average, $\sim$ indicates an oscillating component, $\tilde{q} = \cos(2\theta_{he})$, $j = \frac{1}{2}A_h^2|H_d|^2\frac{1+h^2}{h^2}$, $\tilde{r} = \frac{1}{2}A_h^2|H_d|^2\frac{1-h^2}{h^2}\cdot\cos(2\theta_{hd})$, and $\tilde{u} = A_1A_h|H_d|\frac{1}{h}[(1+h)\cos(\theta_{hd}-\theta) + (1-h)\cos(\theta_{hd}+\theta)]$.

Also, knowing that the average of the oscillating components is zero, (30) can be simplified to

$$\text{THD} = \sqrt{\frac{A_h^2|H_e|^2}{A_1^2 + j}}\cdot 100 \tag{31}$$

which can be put in the following form:

$$\text{THD} = \sqrt{\frac{A_h^2|H_e|^2}{A_1^2}}\cdot\frac{1}{\sqrt{1+\frac{1}{2}\left(\frac{A_1}{A_h}\right)^2|H_d|^2\frac{1+h^2}{h^2}}}\cdot 100$$

$$= \sqrt{\frac{A_h^2|H_e|^2}{A_1^2}}\cdot\Delta\cdot 100 \tag{32}$$

where

$$\Delta = \left(\sqrt{1+\frac{1}{2}\left(\frac{A_1}{A_h}\right)^2|H_d|^2\frac{1+h^2}{h^2}}\right)^{-1}.$$

Consequently, the accuracy is affected by a term Δ that is determined by the relationship A_h/A_1, $|H_d|$ and h. This term has a small impact since the product $(A_h/A_1)^2|H_d|^2 \ll 1$, and then it could be obviated in (32). However, Fig. 9 plots the relationship between Δ and ξ for $h = 3$, 5, 7, and 11 with 5% amplitude with the aim to see its real impact on (32).

Fig. 9 shows that, in the worst case, Δ will impact the THD by an attenuation that is below $2.5\cdot10^{-4}$, for $h = 3$. Then, Δ can be neglected, and it can be assumed that the accuracy is mainly determined by $|H_e|$, i.e., the NF capabilities of the SOGI filter, which can be adjusted by ξ.

Finally, Fig. 10 shows the THD response when $\xi = 0.34$ (1% of error at the fifth harmonic, as shown in Fig. 8) for a simulation in which a 5th harmonic appears at $t = 1$ s, a 7th harmonic appears later at $t = 1.5$ s, and 11th harmonic at $t = 2$ s, which can be visually seen as a staircase perturbation. Each harmonic is of 5% amplitude. In Fig. 10, the measured THD for the fifth harmonic is 4.95% with an 1% error, as expected. The THD for the combination of the 5th and 7th harmonics is 7.02%,

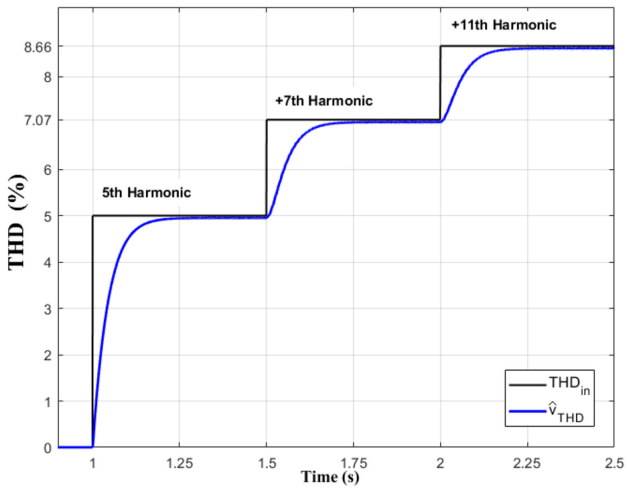

Fig. 10. THD transient response for 5th, 7th, and 11th harmonics with 5% amplitude each. First, a 5th harmonic appears at $t = 1$ s, then a 7th harmonic at $t = 1.5$ s, and an 11th harmonic at $t = 2$ s.

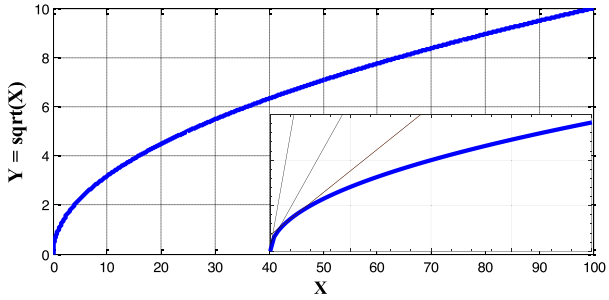

Fig. 11. Plot of the square root function and enlargement for the arguments closer to zero, showing the initial high slopes.

which supposes a 0.72% error. And for the 5th, 7th, and 11th combination, the THD is of 8.60%, which is an error of 0.70%.

D. Impact of the Square Root Nonlinear Operator in the Dynamic Response

The square root $Y = \text{sqrt}(X)$, is a nonlinear operator that is plotted in Fig. 11 for the interval $0 \leq X \leq 100$. As can be seen in the enlargement subplot in the lower right corner of this figure, the square root function presents a high slope for the arguments closer to zero. Nevertheless, the slope progressively decreases as the arguments grow. Therefore, the square root dynamically modifies the gain of the THD measurement system at the event of an input step harmonic perturbation. As a result, the step-up and step-down THD transient responses are unequally affected by this gain.

This fact can be seen in the lower subplot of Fig. 12 that depicts the THD transient response to a single 5th harmonic with 5% amplitude considering the square root operator ($\hat{v}_{\text{THD}}$ signal, in blue line) and not considering it ($\hat{v}_{\text{THD}x}$ signal, in red line). The last one has been scaled in gain and named $\hat{v}_{\text{THD}x}$ in order to match the same steady-state value of $\hat{v}_{\text{THD}}$ and allow their comparison. In this figure, at the step-up at $t = 1$ s, for the initial

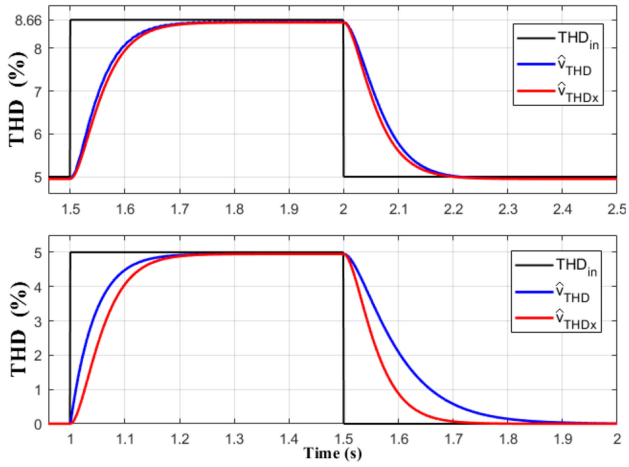

Fig. 12. Response to two different THD step changes: Top: from 5% to 8.66% at $t = 1.5$ s and then back to 5% at $t = 2$ s. Bottom: from 0% to 5% at $t = 1$ s and then back to 0% at $t = 1.5$ s. In blue: THD output. In red: Scaled THD before square root operation.

small values of THD_{in}, the calculated $\hat{v}_{\text{THD}}$ grows up faster than $\hat{v}_{\text{THD}x}$ due to the square root high gain. Nevertheless, the gain slows down as THD_{in} increases, resulting in similar settling times for both signals.

On the other hand, at the step-down at $t = 1.5$ s, as THD_{in} begins to decrease, the signal at $\hat{v}_{\text{THD}}$ reduces at a progressively slower rate, due to the square root operator high gain for low input values, leading to significant differences in their settling times. So, the square root produces a small advancing effect on the step-up and a strong delaying effect on the step-down transient response, which can be clearly seen in the lower subplot. However, this asymmetrical phenomenon disappears for step transients starting from THD levels that are away from zero, which can be seen in the upper subplot of Fig. 12. Note that in this case, there is a permanent fifth harmonic with 5% amplitude and a transient to 8.66%. The THD step perturbation happens at $t = 1.5$ s and disappears at $t = 2$ s. Note that in this case, there is a small difference between $\hat{v}_{\text{THD}}$ and $\hat{v}_{\text{THD}x}$. And that the response at the step-up and step-down transients tend to be symmetrical and $\hat{v}_{\text{THD}}$ is more close to $\hat{v}_{\text{THD}x}$. Note that in the lower subplot of this figure, the square root advances a little bit (0.025 s) the step-up response and strongly delays (0.14 s) the step-down one.

E. Response to Frequency Step Changes and Voltage Sags

The perturbations of the grid like voltage sags and frequency step changes reach the THD using the relation $\mu = (e/A)^2$ in (13). This relationship can be addressed by viewing first the time derivative of the SOGI error, which, from Fig. 2, can be defined as

$$\dot{e} = \dot{v}_i - \dot{v}_d = \dot{v}_i - \hat{\omega} \cdot (2\xi \cdot e - v_q) \tag{33}$$

where $\hat{\omega}$ is the FLL estimated frequency. Hence, assuming steady-state conditions and that there is a frequency step perturbation in the grid, i.e., $v_i = A_1 \sin[(\omega_i + \Delta\omega)t]$, with $\Delta\omega$

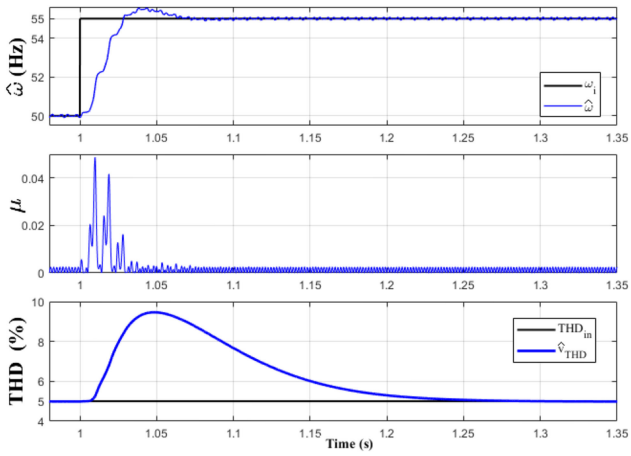

Fig. 13. Transient responses obtained for a frequency step perturbation from 50 to 55 Hz at $t = 1$ s. The grid has a permanent fifth harmonic with 5% amplitude. Top: SOGI-FLL estimated frequency. Middle: μ. Bottom: THD.

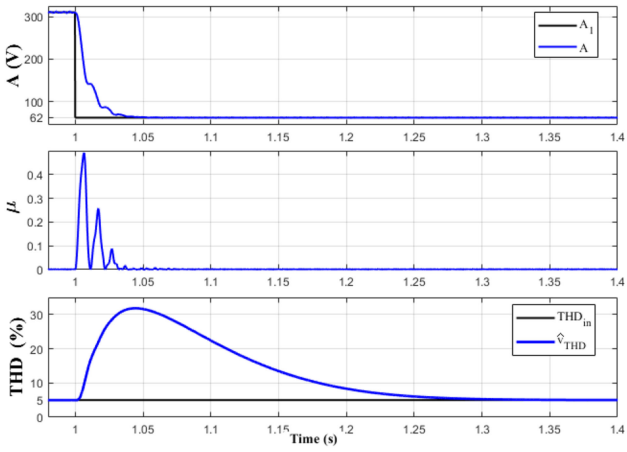

Fig. 14. Transient responses obtained for an 80% depth voltage sag perturbation at $t = 1$ s. The grid has a permanent fifth harmonic with 5% amplitude. Top: SOGI-FLL estimated amplitude voltage. Middle: μ. Bottom: THD.

being the frequency perturbation step size, (31) becomes

$$\dot{e} = (\omega_i + \Delta\omega)\, A_1 \cos\left[(\omega_i + \Delta\omega)\, t\right] - \hat{\omega}\,(2\xi \cdot e - v_q) \quad (34)$$

which determines the perturbation dynamics in $e(t)$. Moreover, the dynamics of $\hat{\omega}$ can be considered as described in [23] and is given as

$$\hat{\omega}\,(s) = \frac{\lambda/2}{s^2 + \xi\omega_n \cdot s + \lambda/2}\Delta\omega\,(s) \quad (35)$$

where $\omega_n = 2\pi 50$ rad/s. On the other hand, using the time derivative of (9) and denoting now A as the estimate of A_1, the perturbation effect in A can be seen as

$$\frac{dA}{dt} = \frac{v_d \cdot \dot{v}_d + v_q \cdot \dot{v}_q}{\left(v_d^2 + v_q^2\right)^{1/2}} = \frac{v_d \cdot \dot{v}_d + v_q \cdot \dot{v}_q}{A} \quad (36)$$

which according to (33), $\dot{v}_d = \hat{\omega}(2\xi \cdot e - v_q)$, and $\dot{v}_d = \hat{\omega} v_d$ gives

$$\frac{dA}{dt} = \frac{2\xi}{A}\hat{\omega} \cdot v_d \cdot e. \quad (37)$$

So, A will be also perturbed by $\hat{\omega}$ and by $e = v_{\text{in}} - v_d$. Therefore, due to the combination of (34) and (37), μ is not straightforward to analyze, but the impact of the perturbation can be assessed using simulations. To this aim, Fig. 13 shows the response to a perturbation from 50 to 55 Hz at $t = 1$ s for a grid with a permanent fifth harmonic of 5% amplitude. The SOGI-FLL and LPF parameters were $\lambda = 55{\cdot}2\ \pi 50$ rad/s^2, $\xi = 0.34$, $n = 2$, and $f_c = 5$ Hz, respectively, which have been designed for achieving a 1% error at a fifth harmonic and a 10% overshoot in the transient response.

As can be seen, in μ, the perturbation causes a burst of pulses that the LPF averages, generating an impulsive-like transient response in the THD. This burst is mainly produced by the quadratic operation over e that turns positive the negative cycles of the error signal.

Fig. 14 depicts the transient response to an 80% depth voltage sag at $t = 1$ s. Note that the same behavior is achieved as in the previous figure, but with a higher THD peak. As a consequence, in both cases, the THD is perturbed transitorily with a transient dynamic that is due to the LPF.

TABLE I
THD MEASURED PEAK AMPLITUDE DUE TO FREQUENCY STEP PERTURBATIONS OF DIFFERENT SIZES

Frequency step size	2 Hz	4 Hz	6 Hz	8 Hz	10 Hz
THD perturbation amplitude (THD-5%)	0.93	3.14	5.86	8.82	11.90

TABLE II
THD MEASURED PEAK AMPLITUDE DUE TO VOLTAGE SAGS OF DIFFERENT DEPTHS

Voltage sag depth size	20%	40%	60%	80%
THD perturbation amplitude (THD-5%)	2.01	7.18	14.81	26.82

The peak size of these perturbations was measured for different frequency and voltage sags with different step sizes and depth levels of 5% that is permanently being measured. Tables I and II summarize these data, which show that the impact of the perturbation in the THD increases naturally with the perturbation magnitude. It can be concluded that for the frequency case, the THD impact follows a quadratic input-to-output relationship as $y = a_2x^2 + a_1x + a_0$, with $a_2 = 0.0035$, $a_1 = 0.97$, and $a_0 = -1.2$. And for the voltage sag, the THD impact can be approximated by a cubic law as $y = b_3x^3 + b_2x^2 + b_1x + b_0$, where $b_3 = 4 \cdot 10^{-5}, b_2 = -0.0017, b_1 = 0.25$, and $b_0 = -2.6$.

The THD impact can be generally mitigated by adjusting the LPF parameters. In the frequency case, it can also be reduced by minimizing the frequency overshoot and by reducing the FLL gain. Fig. 15 illustrates this fact by showing the THD response for the voltage sag case when different filter orders, n, and cutoff frequencies, f_c, are used.

As shown in Fig. 15, an increase in n or decrease in f_c helps reduce the THD perturbation. The most effective parameter is f_c, which reduces the impact on the THD, but producing a longer

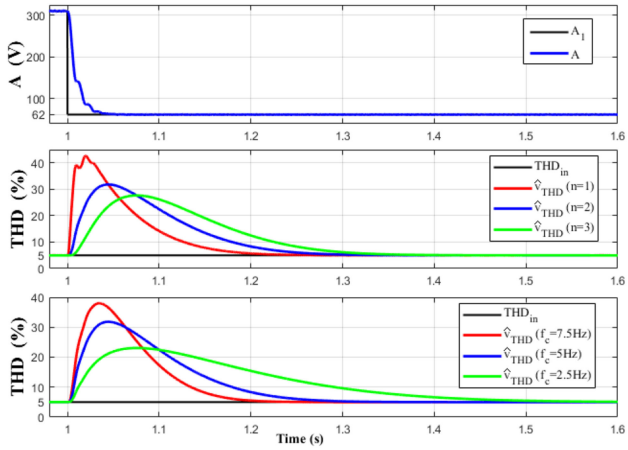

Fig. 15. THD transient responses for an 80% depth voltage sag perturbation at $t = 1$ s. The grid has a permanent fifth harmonic with 5% amplitude. Top: SOGI-FLL estimated amplitude voltage. Middle: THD for different LPF orders, $n = 1$, 2, and 3. Bottom: THD for and different cutoff frequencies, $f_c = 7.5$, 5, and 2.5 Hz.

transient response. The increase in n helps to reduce the impact, but the reduction capacity is lower for $n > 3$.

IV. Experimental Results

Experimental results were first obtained using a Chroma 61501 single-phase programmable ac power source, an analog sensing board prototype wired to a TI Concerto F28M35H52C1 DSP control board, and a personal computer with Code Composer Studio software environment from TI. The Concerto DSP is a dual-core processor that has an advanced risc machine (ARM) Cortex-M3 and a TMS320C28x inside the same chip. The ARM processor is devoted to communication purposes that are not used for this article. The TMS320C28x is a 32-bit floating point processor that runs at 150 MHz clock speed and has 512 kb flash memory. Both processors have a shared RAM memory of 64 kb. The sensing board included a 4-channel and 12-bit DAC7564 digital-to-analog (DAC) chip wired to the DSP control board using a Serial Peripheral Interface communication protocol. The DAC is allowed to display up to four DSP internal variables in real time within a 0–3 V output voltage window. An *R–C* analog LPF with a 1500 Hz cutoff frequency is used in the sensing of the grid voltage to avoid to introduce in the measurement the high-frequency-switching noise of the ac power source. Moreover, a digital high-pass filter and an LPF with 1500 Hz and 1 Hz cutoff frequencies, respectively, were also used in order to avoid the influence of subharmonics and of the DSP high sampling frequency. The experimental results obtained by using the Concerto board are shown in Figs. 17–24.

The comparative experimental results were obtained by measuring the harmonic components using an FFT and by using a second board with a TI's TMS320F28377D 200 MHz, 32-bit floating point DSP. The TMS320F28377D has the same 512 kb flash memory capability as the Concerto board. However, it has more RAM memory, up to 172 kb. This control board is necessary to run properly the FFT routine provided by TI's

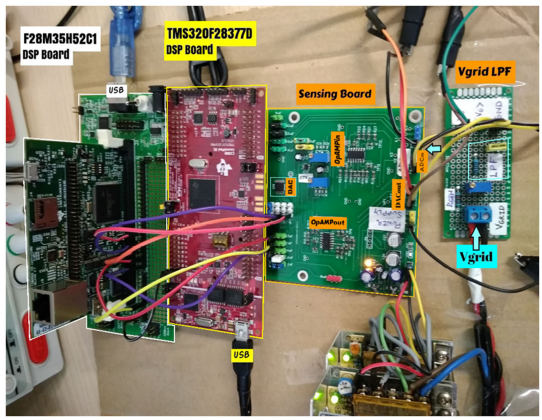

Fig. 16. Experimental setup using two DSP boards and an analog sensing board.

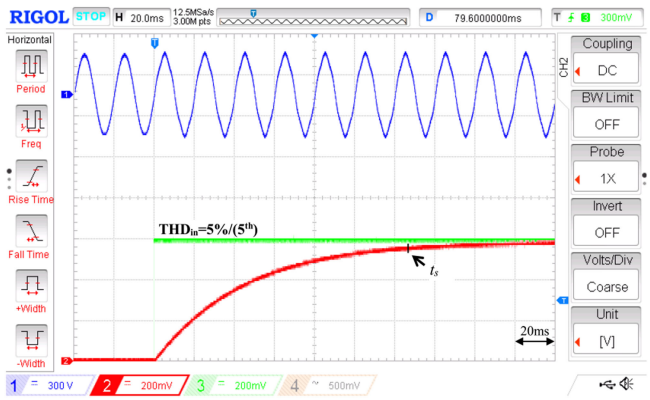

Fig. 17. THD experimental result for grid with a fifth harmonic and 5% amplitude sudden step perturbation. Ch. 1: grid voltage (300 V/div). Ch. 2: THD (200 mV/div or 1.66%/div). Ch. 3: 5% step reference signal (200 mV/div or 1.66%/div).

software library [24], since this routine did not run in the Concerto board due to insufficient RAM memory. This board has a three-channel 12-bit DAC peripheral embedded inside the DSP processor. Fig. 16 depicts a picture of all these boards together. Therefore, the comparison is made from the simultaneous results obtained by the first and second DSP boards. In the comparison, the proposed THD method was implemented in the first DSP, whereas the FFT-based one was implemented in the second DSP. The comparative results are depicted in Figs. 25–29. For both boards, the sampling frequency was 20 kHz, and the SOGI-FLL and the THD measurement diagram blocks were discretized and implemented using the Backward Euler method.

A. Results of the Proposed THD Measurement Method

A periodic fifth-harmonic perturbation of 5% amplitude was programmed in the ac power source with a 220 V(rms)/50 Hz fundamental voltage. Fig. 17 shows the ac power source voltage in channel 1, the obtained THD measurement in channel 2, and a step 5% THD artificial signal in channel 3 generated to contrast with the measurement. The SOGI and LPF parameters were $\xi = 0.7$, $\omega_o = 2\pi 50$ rad/s, $n = 2$, and $f_c = 5$ Hz. The signals in channels 2 and 3 were amplified to fit them to the 3 V DAC

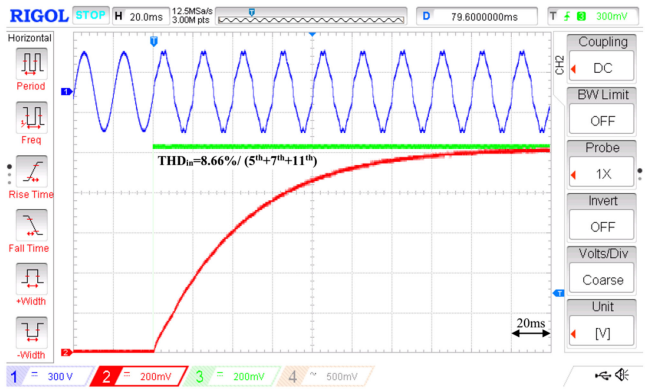

Fig. 18. THD experimental result for grid with a combination of 5th, 7th, and 11th harmonics (5% amplitude each) sudden step perturbation. Ch. 1: grid voltage (300 V/div). Ch. 2: THD (200 mV/div or 1.66%/div). Ch. 3: 8.66% step reference signal (200 mV/div or 1.66%/div).

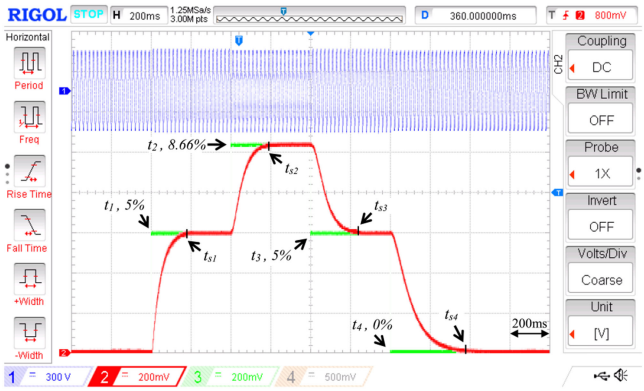

Fig. 21. THD experimental results for sequential THD perturbations using 5th, 7th, and 11th harmonics: from 0 to 5% at t_1, from 5% to 8.66% at t_2, back from 8.66 to 5% at t_3, and back from 5 to 0% at t_4. Ch. 1: grid voltage (300 V/div). Ch. 2: THD (200 mV/div or 1.66%/div). Ch. 3: step reference signals, t_1 and $t_3 = 5\%$, $t_2 = 8.77\%$, and $t_4 = 0\%$ (200 mV/div or 1.66%/div).

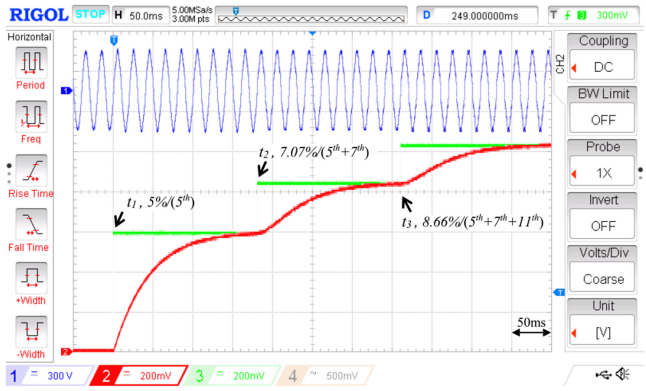

Fig. 19. THD experimental results for sequential perturbations of 5th, 7th, and 11th harmonics that were consecutively activated after 0.21 s each. Ch. 1: grid voltage (300 V/div). Ch. 2: THD (200 mV/div or 1.66%/div). Ch. 3: step reference signals, 5% at t_1, 7.07% at $t_2 = 7.07\%$, and 8.66% at t_3 (200 mV/div or 1.66%/div).

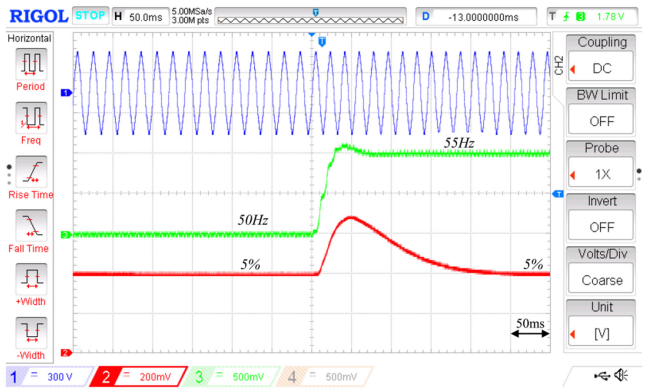

Fig. 22. THD experimental results for frequency step perturbation from 50 to 55 Hz. The grid has a permanent fifth-harmonic distortion with a 5% amplitude. Ch. 1: grid voltage (300 V/div). Ch. 2: THD (200 mV/div or 2.5%/div). Ch. 3: estimated frequency (500 mV/div or 2.5 Hz/div).

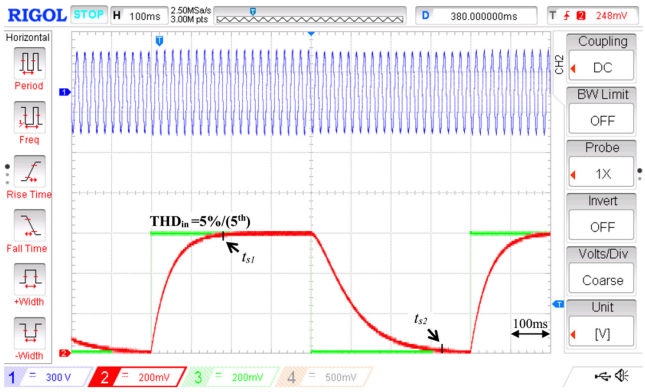

Fig. 20. Experimental results of the THD measurement method for a periodic perturbation of a fifth harmonic of 5% amplitude. Ch. 1: grid voltage (300 V/div). Ch. 2: THD (200 mV/div or 1.66%/div). Ch. 3: 5% step reference signal (200 mV/div or 1.66%/div).

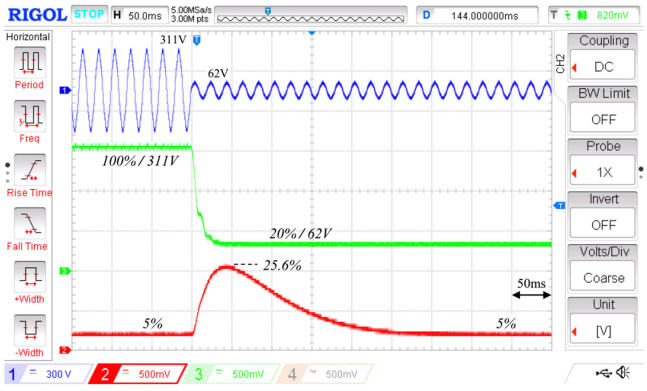

Fig. 23. THD experimental results for 80% depth voltage sag. The grid has a permanent fifth harmonic distortion with a 5% amplitude. Ch. 1: grid voltage (300 V/div). Ch. 2: THD (500 mV/div or 12.5%/div). Ch. 3: estimated amplitude voltage (500 mV/div or 100 V/div).

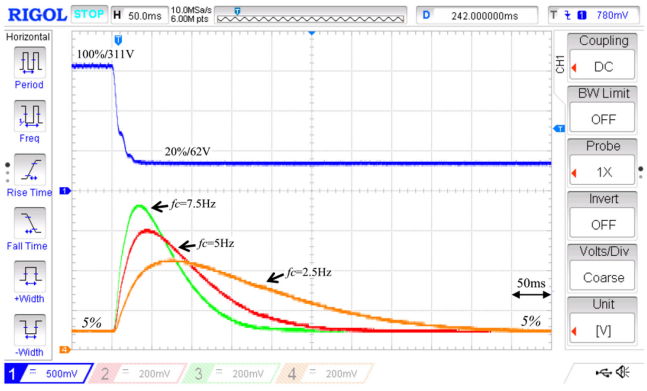

Fig. 24. THD experimental results for 80% depth voltage sag. The grid has a permanent fifth harmonic distortion with a 5% amplitude. Ch. 1: estimated amplitude voltage (500 mV/div or 100 V/div). Ch. 2, Ch3, and Ch4: THD for $f_c = 5$ Hz, 7.5 Hz, and 2.5 Hz, respectively (200 mV/div or 10%/div).

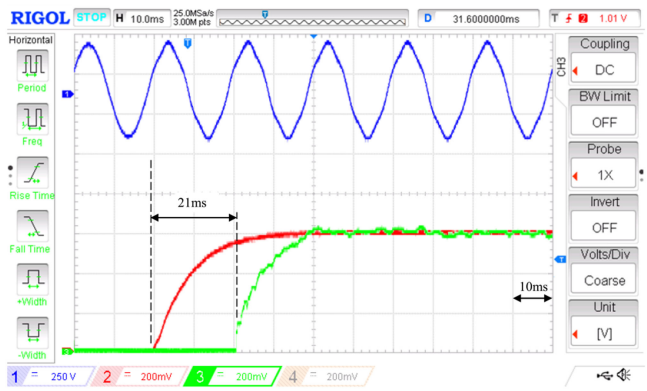

Fig. 27. Detailed (10 ms/div) experimental results for FFT-based THD ($N = 128$) and proposed THD methods for a periodic perturbation of a fifth harmonic of 5% amplitude. Ch. 1: grid voltage (250 V/div). Ch. 2: THD (200 mV/div or 1.66%/div). Ch. 3: FFT-based THD (200 mV/div or 1.66%/div).

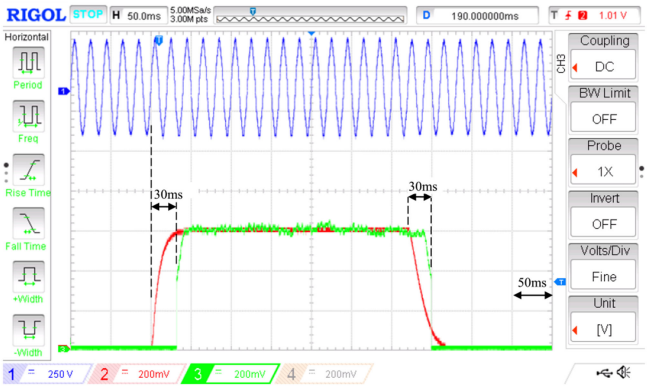

Fig. 25. Experimental results for FFT-based THD ($N = 64$) and proposed THD methods for a periodic perturbation of a fifth harmonic of 5% amplitude. Ch. 1: grid voltage (250 V/div). Ch. 2: THD (200 mV/div or 1.66%/div). Ch. 3: FFT-based THD (200 mV/div or 1.66%/div).

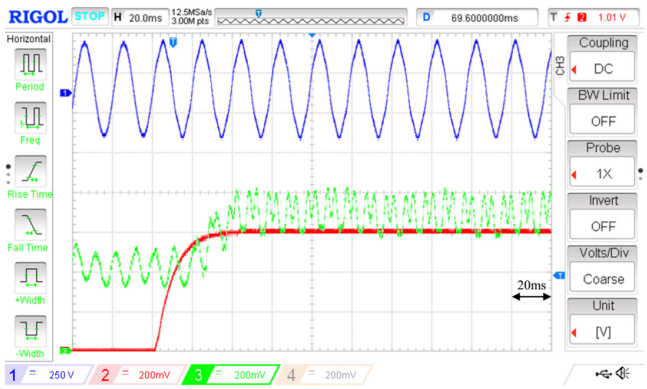

Fig. 28. Experimental results for FFT-based THD ($N = 64$) and the proposed THD methods for 51 Hz grid frequency and a periodic perturbation of a fifth harmonic of 5% amplitude. Ch. 1: grid voltage (250 V/div). Ch. 2: THD (200 mV/div or 1.66%/div). Ch. 3: FFT-based THD (200 mV/div or 1.66%/div).

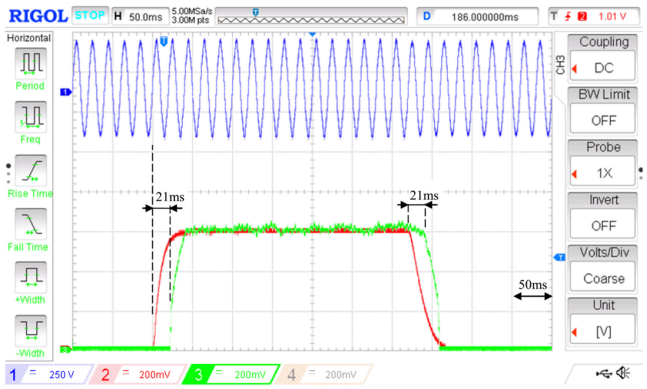

Fig. 26. Experimental results for FFT-based THD ($N = 128$) and proposed THD methods for a periodic perturbation of a fifth harmonic of 5% amplitude. Ch. 1: grid voltage (250 V/div). Ch. 2: THD (200 mV/div or 1.66%/div). Ch. 3: FFT-based THD (200 mV/div or 1.66%/div).

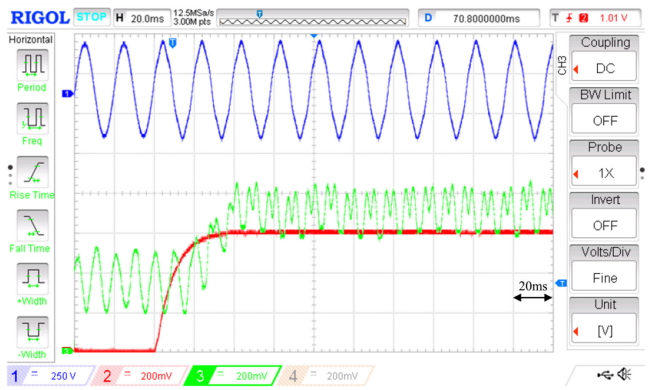

Fig. 29. Experimental results for FFT-based THD ($N = 128$) and proposed THD methods for a 51 Hz grid frequency and a periodic perturbation of a fifth harmonic of 5% amplitude. Ch. 1: grid voltage (250 V/div). Ch. 2: THD (200 mV/div or 1.66%/div). Ch. 3: FFT-based THD (200 mV/div or 1.66%/div).

output window, so that the vertical axis gains were 200 mV/div, which in this case corresponded to 1.66%/div.

In the same manner, Fig. 18 shows the experimental result for a simultaneous 5th-, 7th- and 11th-harmonic perturbation of 5% amplitude each, which corresponds to an input THD step perturbation of 8.66%. Note that in Figs. 17 and 18, the THD is close to the expected 5% and 8.66% values. In fact, these THDs reach the steady-state values of 4.8% and 8.45%, respectively, which correspond to the expected ones for the designed ξ parameter (see Figs. 5 and 6). The measured settling time in Fig. 18 considering a 2% error criterion regarding the THD steady-state is $t_s = 130$ ms, which also corresponds to the expected dynamics.

The SOGI damping factor was reduced to $\xi = 0.34$ in order to increase the accuracy of the measurement to a 1% error for a fifth harmonic using the plots shown in Fig. 8. A sequence of 5th-, 7th-, and 11th-harmonic perturbations of 5% amplitude each was programmed in the ac power source. The 5th harmonic happened first at t_1, followed by a 7th harmonic after 0.21 s, labeled as t_2, and an 11th harmonic after 0.42 s, labeled as t_3. Then, the grid had a THD sequence perturbation of 5%, 7.07%, and 8.66%, respectively. Fig. 19 depicts the experimental result, which clearly shows that the THD is accurate. The measured THDs from the inner DSP variables were 4.95%, 7.02%, and 8.60%, respectively, which coincide with Fig. 10.

Next, Fig. 20 depicts the result for a periodic perturbation of a single fifth harmonic with 5% amplitude in order to see the impact of the square root nonlinear operator on the dynamic response. In Fig. 20, two settling times have been labeled: t_{s1}, and t_{s2}. Note how t_{s2}, at the step-down transient, is much larger than t_{s1}, which denotes the same behavior as explained in Section III-C. Moreover, other sequential THD step perturbations were used starting first from 0% to 5% THD using a 5th harmonic at t_1, then from 5% to 8.66% using additional 7th and 11th harmonics at t_2, then back from 8.66% to 5% at t_3, and finally back from 5% to 0% at t_4. Fig. 21 depicts the experimental response. As shown in the figure, the transient responses at t_1 and t_2 have a similar settling time (t_{s1} and t_{s2}). However, the transient at t_3 is a bit larger than the previous ones, and the transient at t_4 is visibly the longest one, as illustrated in Section III-C.

Figs. 22 and 23 depict the response to a frequency step perturbation from 50 to 55 Hz and to an 80% depth voltage, respectively. The SOGI-FLL and LPF parameters were $\xi = 0.7$, $\lambda = 55{\cdot}2\pi 50$ rad/s^2, $\xi = 0.34$, $n = 2$, and $f_c = 5$ Hz. Note that in Fig. 22, the THD peak amplitude for 5% is 3.6% and that the voltage sag in Fig. 23 induces a THD peak amplitude of 26.5%, which coincide with the results shown in Figs. 13 and 14, respectively.

Finally, Fig. 24 shows the results using an LPF with different cutoff frequencies, $f_c = 7.5$, 5, and 2.5 Hz, and grid with an 80% depth voltage sag. Note that the results coincide with the one shown in Fig. 15.

B. Comparison With the FFT-Based THD

An alternative online FFT-based THD measurement method was implemented on a second board with a TMS-320F28377D 200 MHz DSP with more RAM capability (172 kb). The FFT was computed using the subroutines of the optimized library provided by TI [24]. The FFT can be applied on a digitalized signal with $N = 64$, 128, 256, 512, or 1024 samples per period and requires the following memory resources: a 2N-size input buffer for holding a minimum of two periods of the signal, two 2N-size buffers for intermediate variables, an N-size buffer for coefficients, and an (N/2+1)-size output buffer to provide the magnitude of the fundamental and harmonics components. The sampling time T_s is determined as $T_s = 1/(50N)$ s.

TABLE III
SAMPLING TIME T_s AND MEASURED COMPUTATION TIME FOR THE FFT-BASED THD, ACCORDING TO THE NUMBER OF SAMPLES N

N	64	128	256	512	1024
T_s (μs)	312.5	156.25	78.12	39.06	19.53
Computation time (μs)	25.2	50	102.2	214	454

The computational burden of the employed FFT routines was measured using a digital output pin of the DSP. The measurements were made considering a 50 Hz grid voltage signal and are shown at Table III. The results indicate that the FFT routines can only be applied for $N = 64$ and 128, since only in these cases, the time needed to compute the FFT is lower than the required sampling time T_s. The time needed for $N = 256$, 512, and 1024 is higher than T_s and, thus, the FFT cannot be processed at every sample by the DSP. Therefore, the comparison between the two THD measurement methods will only be made for $N = 64$ and $N = 128$.

The THD is computed according to (1) in the following order.

1) The FFT routines presented in [24] are applied once the input buffer is filled with samples of the grid voltage.
2) The sum of the squares of the harmonics provided at the output buffer is computed using a software loop.
3) The THD is calculated applying the square root operation and then dividing by the fundamental.
4) The content of the input buffer is displaced one position to leave space for holding the next sample at the next iteration of this process.

The FFT library provides information about the number of processor cycles needed for executing the routines [24]. These data have been used here for estimating the burden required to compute the FFT-based THD, which is given in Table IV. This table also shows the number of 32-bit floating point RAM variables required for the computation. In the same way, the computational burden of the proposed THD method following the schemes depicted in Figs. 2 and 4 has been measured, using the Concerto DSP board and the tools of Code Composer Studio software [25]–[29]. The results are listed in Table V and show that the computational burden for the proposed THD method is considerably lower than the FFT-based one and needs fewer RAM memory resources. The time required for computing the proposed THD method has also been measured and amounts to 4.3 μs.

The comparison between the FFT-based THD and the proposed THD measurement method is made for the detection of a periodic fifth harmonic distortion. In the test, the cutoff

TABLE IV
COMPUTATIONAL BURDEN IN PROCESSOR CYCLES (C) FOR THE FFT-BASED THD

N	64	128
FFT routines (c)	2780	5926
Sum of squares of harmonics (c)	236	460
Square root and division (c)	68	68
Buffer displacement (c)	261	517
Total (c)	**3393**	**7019**
Number of 32-bit float RAM variables		
Input buffer	128	256
Output buffer	64	128
Coefficients buffer	64	128
Magnitude buffer	33	65
Other	4	4
Total	**293**	**581**

TABLE V
COMPUTATIONAL BURDEN IN PROCESSOR CYCLES (C) FOR THE PROPOSED THD METHOD

Block description	Cycles (c)
SOGI	149
A^2 and saturation	24
FLL	49
e^2, division and multiplication by 2	32
Square root and multiplication by 100	35
Second-order LPF	65
Total	**354**
Number of 32bit float RAM variables	**29**

frequency of the THD LPF is chosen as $f_c = 20$ Hz. Figs. 25 and 26 depict the results for $N = 64$ and $N = 128$, respectively.

As can be seen in Figs. 25 and 26, the transient response of the FFT-based THD has a delay that is different in each case.

In Fig. 25, for $N = 64$, the delay is 30 ms, and in Fig. 26, for $N = 128$, the delay is 21 ms. Therefore, the proposed THD method shows to be faster and less sensitive to noise than the FFT-based one. Fig. 27 shows another scope capture as shown in Fig. 26 but with more details (10 ms/div). Moreover, the response can be accelerated by increasing the LPF cutoff frequency but at the expense of extra-noise at the THD measurement. Note also that the FFT for $N = 128$ has less noise than for $N = 64$, which is a general characteristic of the FFT routine, that achieves more accuracy with the increase in the number of signal samples.

Furthermore, the computation of the FFT provides inaccurate results when T_s deviates from its specified value or when the grid frequency moves away from the nominal frequency. This situation has been programmed and tested in the experiments, showing problems only in the FFT-based THD method. Figs. 28 and 29 show the comparative results for the FFT-based THD for $N = 64$ and 128, respectively, when the operating grid frequency is 51 Hz. Note that in these two figures, the FFT-based THD measurement method is always inaccurate and provides results with nonlinear oscillations and dc offset errors. Moreover, the greater the frequency deviation, the more the inaccuracy in the THD measurement increases. Note that for the proposed THD method, this problem does not exist.

In summary, the proposed THD method is more accurate, requires few computational resources, achieves faster results, and has less problems than the FFT-based THD. This points out to its viability for measuring the THD and for being implemented in standard and low-cost DSP processors in the different kinds of applications suggested in Section I. However, it is important to remark that the method uses two LPF to stablish a clear lower (subharmonic) and higher (maximum harmonic to be considered) boundaries to the input signal. Theses filters are important to avoid the effect of subharmonics and of extra switching noise in the measurement.

V. CONCLUSION

This article proposes a simple method for obtaining the THD of the grid with a small computational burden, requiring of few math operations, an LPF, and a square root that can be easily implemented into some standard and low-cost DSP processors. The THD is computed using the SOGI-FLL approach that provides the fundamental and harmonic components, but can also be implemented with other grid monitoring solutions, such as PLL or ANF. The fundamental component amplitude is obtained in this case from the SOGI orthogonal outputs and the harmonic components through the NF transfer function behavior of the SOGI error signal. The accuracy of the system was analyzed, and it was concluded that it relies mainly on the NF capability of the SOGI filter, which is determined by the SOGI damping factor parameter. The THD dynamic response corresponds predominantly to that of the LPF and is determined by its cutoff frequency f_c. However, the dynamic is affected by the nonlinearity of the square root operator in the THD, which impact the dynamic response with asymmetric effects on the step-up and step-down transient responses. The worst case effects happen at the step-down transient response, when the THD is small and close to zero. The behavior of the method in front of grid perturbations, such as frequency steps and voltage sag perturbations, was also analyzed. These perturbations induce a burst of impulses at the THD input that is filtered out by the LPF and generate an impulse-like perturbation. This impulsive perturbation disappears after a short time determined by the magnitude of the perturbation and by the LPF design parameters. Simulations and experimental results were provided that corroborate the performance of the system in terms of accuracy, dynamic response, and robustness in front of grid perturbations. Moreover, an experimental comparison with an FFT-based THD is made, showing that the proposed method is faster and has a very small computational burden regarding the FFT one. Additionally, the proposed THD method provides a measurement with less noise and is robust in front of grid frequency variations from nominal frequency.

ACKNOWLEDGMENT

This project was funded by the Deanship of Scientific Research (DSR) at King Abdulaziz University, Jeddah, under Grant D-185-135-1440. The authors, therefore, acknowledge with thanks DSR for technical and financial support.

REFERENCES

[1] R. C. Dugan, M. F. Mcgranaghan, S. Santoso, and H. W. Beaty. *Electrical Power Systems Quality*, 3rd ed. New York, NY, USA: McGraw-Hill, 2002.

[2] A. Kusko and M.C. Thompson. *Power Quality in Electrical Systems*. New York, NY, USA: McGraw-Hill, 2007.

[3] IEEE Recommended Practices and Requirements for Harmonic Control in Electric Power Systems, IEEE Std 519-1992, 1993.

[4] G.E. Mog and E.P. Ribeíro, "Total harmonic distortion calculation by filtering for power quality monitoring," in *Proc. IEEE Transm. Distrib. Conf. Exp., Latin Am.*, 2004, pp. 1–4.

[5] D. Schmilovitz, "On the definition of total harmonic distortion and its effect on measurement interpretation." *IEEE Trans. Power Del.*, vol. 20, no. 1, pp. 526–528, Jan 2005.

[6] I.V. Blagouchine and E. Moreau, "Analytic method for the computation of the total harmonic distortion by the Cauchy method of residues," *IEEE Trans. Commun.*, vol. 59, no. 9, pp. 2478–2491, Sep. 2011.

[7] C. Muresan, F. Dragan, and V.D Zaharia, "Total harmonic distortion computation in nonsynchronized sampling condition," *Acta Electrotehnica*, vol. 52, no. 2, pp. 114–118, 2011.

[8] R. Ingale, "Harmonic analysis using FFT and STFT," *Int. J. Signal Process, Image Process. Pattern Recognit.*, vol. 7, no. 4, pp. 345–362, 2014.

[9] N. Farokhina, H. Vadizadeh, S.H. Fathi, and F. Anvariasl, "Calculating the formula of line-voltage THD in multilevel inverter with unequal dc sources," *IEEE Trans. Ind. Electron.*, vol. 58, no. 8, pp. 3359–3372, Aug. 2011.

[10] B. M. Antic, Z. L. Mitrovic, and V. V. Vujicic, "A method for harmonic measurement of real power grid signals with frequency drift using instruments with internally generated reference frequency," *Meas. Sci. Rev.*, vol. 12, no. 6, pp. 277–285, 2012.

[11] K. Sajjad, G. Kalsoom, and A. Mughal, "Simplified THD measurement and analysis for electronic power inverters," in *Proc. IEEE Int. Bhurban Conf. Appl. Sci. Technol.*, 2015, pp. 186–191.

[12] R. Abdikarimuly, Y.L. Familiant, A. Ruderman, and B. Reznikov, "Calculation of current total harmonic distortion for a single-phase multilevel inverter with LCL-filter," in *Proc. IEEE Int. Power Electron. Motion Control Conf.*, 2016, pp. 63–68.

[13] F. C. Alegria, "Precision of the sine fitting-based total harmonic distortion estimator," *Metrol. Meas. Syst.*, vol. 23, no. 1, pp. 37–46, 2016.

[14] D. Yazdani, A. Bakhshai, and P. K. Jain, "A three-phase adaptive notch filter-based approach to harmonic/ reactive current extraction and harmonic decomposition," *IEEE Trans. Power Electron.*, vol. 25, no. 4, pp. 914–923, Apr. 2010.

[15] B. Burger and A. Engler, "Fast signal conditioning in single phase systems," in *Proc. Eur. Power Electron. Appl. Conf.*, 2001.

[16] P. Rodriguez, A. Luna, M. Ciobotaru, R. Teodorescu, and F. Blaabjerg, "Advanced grid synchronization system for power converters under unbalanced and distorted operating conditions," in *Proc. 32nd Annu. Conf. IEEE Ind. Electron.*, 2006, pp. 5173–5178.

[17] J. Matas, M. Castilla, J. Miret, L. G. de Vicuna, and R. Guzman, "An adaptive prefiltering method to improve the speed/accuracy tradeoff of voltage sequence detection methods under adverse grid conditions," *IEEE Trans. Ind. Electron.*, vol. 61, no. 5, pp. 2139–2151, May 2014.

[18] J. Matas, H. Martin, J. De La Hoz, A. Abusorrah, Y. Al-Turki, and M. Al-Hindawi, "A family of gradient descent grid frequency estimators for the SOGI filter," *IEEE Trans. Power Electron.*, vol. 33, no. 7, pp. 5796–5810, Jul. 2018.

[19] M. Ciobotaru, R. Teodorescu, and F. Blaabjerg, "A new single-phase PLL structure based on second order generalized integrator," in *Proc. IEEE Power Electron. Spec. Conf.*, 2006, pp. 1–6.

[20] M. Karimi-Ghartemani and M. R. Iravani, "A nonlinear adaptive filter for online signal analysis in power systems applications," *IEEE Trans. Power Del.*, vol. 17, no. 2, pp. 617–622, Apr. 2002.

[21] M. Karimi-Ghartemani, *Enhanced Phase-Locked Loop Structures for Power and Energy Applications*. Piscataway, NJ, USA: IEEE Press, 2014.

[22] S. Golestan, J.M. Guerrero, and J.C. Vasquez, "Single-phase PLLs: A review of recent advances," *IEEE Trans. Power Electron.*, vol. 32, no. 12, pp. 9013–9030, Dec. 2017.

[23] S. Golestan, E. Ebrahimzadeh, J. M. Guerrero, and J.C. Vasquez, "An adaptive resonant regulator for single-phase grid-tied VSCs," *IEEE Trans. Power Electron.*, vol. 33, no. 3, pp. 1867–1873, Mar. 2018.

[24] FPU DSP Software Library User's Guide, Texas Instruments, Dallas, TX, USA, 2015.

[25] Code Composer Studio Users Guide, Texas Instruments, Dallas, TX, USA, 2019. [Online]. Available: http://www.ti.com/tool/CCSTUDIO

[26] TMS320C28x Floating Point Unit and Instruction Set Reference Guide, Texas Instruments, Dallas, TX, USA, 2015.

[27] TMS320C28x CPU and Instruction Set Reference *Guide*, Texas Instruments, Dallas, TX, USA, 2015.

[28] TMS320C28x FPU Primer, Texas Instruments, Dallas, TX, USA, 2009.

[29] C28x FPU Fast RTS Library, Texas Instruments, Dallas, TX, USA, 2008.

José Matas received the B.S., M.S., and Ph.D. degrees in telecommunications engineering from the Technical University of Catalonia, Barcelona, Spain, in 1988, 1996, and 2003, respectively.

From 1988 to 1990, he was an Engineer with a consumer electronics company. Since 1990, he has been an Associate Professor with the Department of Electronic Engineering, Technical University of Catalonia, Spain. In 2017, he enrolled to the Department of Electrical Engineering. His research interests include the areas of power electronics, nonlinear control, power quality, renewable energy systems, smart grid, and microgrids.

Helena Martín received the B.Sc. and M.Sc. degrees in electronic engineering from the Technical University of Catalonia (UPC) and the Ph.D. degree in industrial engineering in 1994, 1997, and 2007, respectively.

She is currently an Associate Professor with the Department of Electric Engineering, Technical University of Catalonia. Her research interests include microgrids control, optimal management, and energy policy for microgrids with renewable energy generation.

Jordi de la Hoz received the B.Sc. degree in electrical engineering, the M.Sc. degree in industrial electronics and automatic control, and the Ph.D. degree in industrial engineering all from the Technical University of Catalonia (UPC), in 1998, 2002, and 2009, respectively.

Since 2001, he has been with the Electrical Engineering Department, UPC. His main research interest includes the analysis of the impact that the regulatory frameworks have on the development, design, and management of renewable energy systems (including microgrids).

Abdullah Abusorrah (M'08–SM'14) received the B.S. and M.S. degrees in electrical engineering from the King Abdulaziz University, in 1994 and 2002, respectively, and the Ph.D. degree in electrical engineering from the University of Nottingham, U.K., in 2007.

He is currently an Associate Professor with the Department of Electrical and Computer Engineering, King Abdulaziz University, where he is also the Head of Renewable Energy Research Group. His research interests include power quality, smart grid, and system analyses.

Yusuf Al-Turki (M'90–SM'17) received the Ph.D. degree in power systems from the University of Manchester, U.K., in 1985.

Since 1999, he has been a Professor with the Department of Electrical and Computer Engineering, King Abdulaziz University, Saudi Arabia, where he is also the Dean of Research. His research interests include system modeling, power system dynamics, renewable energy, and microgrids.

Hamed Alshaeikh received the B.S. and M.S. degrees in electrical engineering power-machine from King Abdulaziz University, Jeddah, Saudi Arabia, in 2009 and 2017, respectively.

In 2009, he joined Commissioning Services Department, Saudi Electricity Company, as an Electrical Engineer responsible for pre-energization testing and commissioning for old and new electrical substations range from 380–13.8 kV. In 2015, he joined Siemens Ltd., Riyadh, Saudi Arabia, as a Project Manager for protection system, RTU, and substation automation.